Pergamon

Int. J. Solids Structures Vol. 35, No. 16, pp. 1851–1861, 1998

0020–7683/98 $19.00 + .00

PII: S0020–7683(97)00158–3

SIZE-EFFECTS INDUCED BIFURCATION PHENOMENA DURING MULTIPLE COHESIVE CRACK PROPAGATION

FABRIZIO BARPI and SILVIO VALENTE
Dipartimento di Ingegneria Strutturale, Politecnico di Torino, Corso Duca degli Abruzzi 24, 10129 Torino, Italy

(*Received* 14 *May* 1996; *in revised form* 21 *May* 1997)

Abstract—The nonlinear behavior of concrete-like materials in tension is characterised by strain-softening. Phenomena involving the localisation of strain caused by strain softening can be analysed accurately through the so-called "cohesive crack model" which uses the length of the fictitious crack as a control variable. In this approach, the length of the process zone is not fixed and the ratio between this length and the length of the specimen decreases with increasing size-scale. This phenomenon is evident even for small changes in size. It can explain why, in four point shear test, a critical size is observed, below which a secondary crack starts to propagate. This is a size-related phenomenon of bifurcation of equilibrium path, which is predicted by the cohesive crack model and confirmed experimentally. The theoretical results obtained by means of the cohesive crack model involving two cracks are in good agreement with experimental results. © 1998 Elsevier Science Ltd.

1. INTRODUCTION

Brittle and disordered materials such as concrete, rock, ceramics, etc. contain a large number of flaws and micro-cracks. When these materials are subjected to high tensile stresses, an interaction takes place in the process of microcrack growth. This phenomenon gives rise to strain localisation within a very narrow band, where energy dissipation occurs, while the material outside this zone behaves in a linear-elastic mode. According to the concepts of continuum mechanics, it can be stated that in this band, referred to as process zone, the bearing capacity is reduced ($d\sigma < 0$) as a consequence of an anelastic increment in strain ($d\varepsilon > 0$).

This phenomenon, called strain-softening, represents a violation of the stability postulate $d\sigma\, d\varepsilon \geqslant 0$ (Drucker, 1988) and, therefore, makes the classical theory of plasticity inapplicable. The consequences of this violation were investigated by many authors (Maier, 1971; Maier *et al.*, 1973); they showed that, even in the absence of geometric instability effects, the following phenomena may occur:

- loss of stability, in controlled load conditions (snap-through),
- loss of stability, in controlled displacement conditions (snap-back),
- bifurcation of the equilibrium path,
- loss of uniqueness of the equilibrium path,
- pathological dependence of the results on the type of mesh used in the numerical analysis.

It is important to point out that whilst the material in the process zone is in a post-critical stage, the structure as a whole may still be in a pre-critical stage not having yet reached the maximum load. For this reason, despite the difficulties mentioned above, strain-softening must be taken into account as an indispensable step to provide a better explanation of many mechanical phenomena of interest for engineering purposes. For this reason, the cohesive crack model was initially proposed in order to overcome some of the shortcomings encountered when applying plasticity theory to the study of cracking in metals (Barenblatt, 1959; Dugdale, 1960). More recently, one modified version of the cohesive model called fictitious crack model was proposed (Hillerborg *et al.*, 1976). The latter model was applied

primarily to concrete-like materials and was numerically implemented through a finite element program.

Subsequently, by applying the cohesive model to Mode I (Carpinteri, 1985; Carpinteri, 1989), and mixed-mode problems (Carpinteri and Valente, 1988; Carpinteri *et al.*, 1992; Carpinteri *et al.*, 1993; Bocca *et al.*, 1991), it proved possible to account for the transition from ductile to brittle behavior as a function of varying specimen size alone, the material and all geometric ratios being the same.

In this investigation, the cohesive model is applied to the case of two cracks propagating simultaneously.

2. THE COHESIVE MODEL APPLIED TO THE PROPAGATION OF TWO CRACKS

The cohesive model rests on the assumption that, as an extension of the real crack, a fictitious crack (also referred to as process zone) is formed, where the material, albeit damaged, is still able to transfer stresses which are decreasing functions of the relative displacement discontinuity, as shown in Fig. 1.

It may, therefore, be stated that the cohesive model is based on a double constitutive law; one is applied to the undamaged material and it is the classical linear-elastic relationship between stresses and strains (Fig. 2a), while the other is applied to the process zone and may give rise to two conditions (Fig. 2b):

$$\sigma_c = \sigma_u\left(1 - \frac{w_n}{w_{nc}}\right) \quad \text{for } \dot{w}_n > 0 \quad \text{(softening)} \tag{1}$$

$$\sigma_c \leqslant \sigma_u\left(1 - \frac{w_n}{w_{nc}}\right) \quad \text{for } \dot{w}_n = 0 \quad \text{(local rigid unloading)} \tag{2}$$

where σ_c is the closing stress and w_n is the related opening displacement (the dot denoting derivation with respect to time). The tangential components acting on the fictitious crack are neglected ($\tau_c = 0$).

This is a first approximation hypothesis which is sufficient, however, to interpret many laboratory tests. With the restraint and loading arrangements considered in this investigation, it has been found that in numerical simulations, conditions (1) and (2) are never simultaneously present at two points of a single crack. In other words, it can be stated that, for each growth step of the two cracks, one of the following may occur:

(a) both cracks grow,
(b) the first crack grows, while second does not, even though it opens,

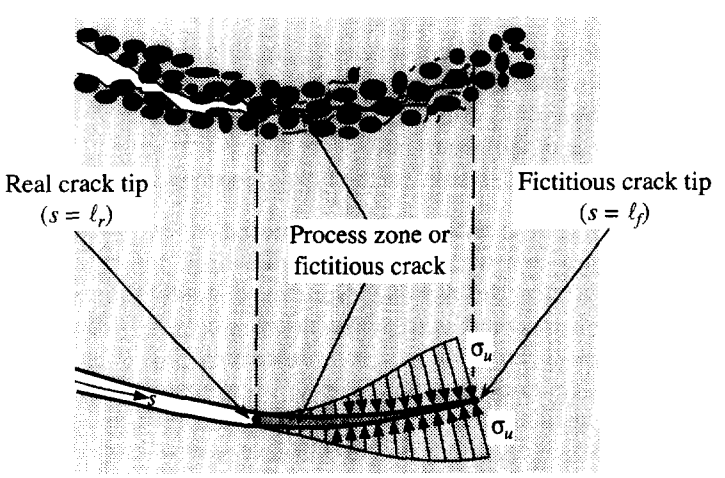

Fig. 1. The cohesive model represents the process zone as a fictitious extension of the real crack.

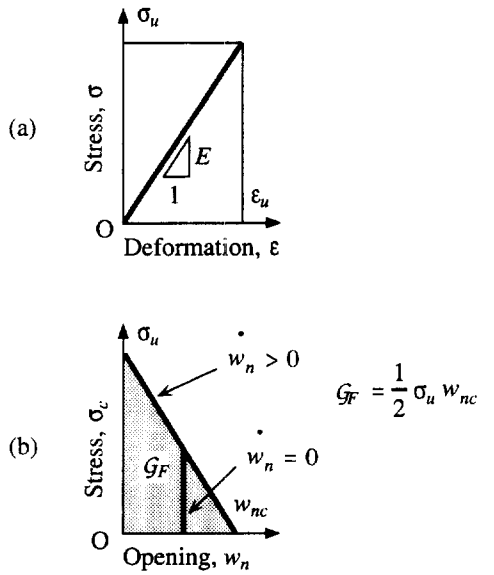

Fig. 2. Double constitutive law: (a) for the undamaged material; (b) for the fictitious crack.

(c) the second crack grows, while first does not, even though it opens,
(d) the first crack grows and the second undergoes rigid unloading,
(e) the second crack grows and the first undergoes rigid unloading.

The hypothesis of rigid unloading on the part of both cracks has been ruled out, as the restraint and loading conditions employed were specially designed to ensure specimen splitting.

During the analysis, more than one of the five solutions described above (a–e) may turn out to be admissible from the static and kinematic viewpoints. If this is so, one of the possible solutions is chosen according to the maximum energy release rate criterion, which is also used in linear-elastic fracture mechanics (Nemat-Nasser *et al.*, 1980; Nguyen, 1987) and is a direct consequence of the basic laws of thermodynamics (Bazant and Cedolin, 1991).

Since both the constitutive laws illustrated in Fig. 2 are linear, by using the finite element method and assuming the n nodal incremental displacements $\Delta\mathbf{u}$ as the unknown quantities, it is possible to impose the equilibrium condition through the principle of virtual work, as follows (Carpinteri and Valente, 1988; Carpinteri *et al.*, 1993; Bocca *et al.*, 1991):

$$\mathbf{L}_i^{(j)}\,\Delta\mathbf{u}_i^{(j)} = \Delta\lambda_i^{(j)}\,\mathbf{F} \tag{3}$$

where

- superscript j stands for the jth step of the external cycle. At each step, either one or both fictitious cracks grow,
- subscript i stands for the ith step of the internal iterative cycle. At each step, one of the real cracks grows,
- $\mathbf{L}_i^{(j)}$ is the path dependent symmetrical $(n \times n)$ matrix assembled by bringing together the contributions from both constitutive laws. It depends on the real crack length (ℓ_r) and fictitious crack length (ℓ_f) of both cracks,
- $\mathbf{F}$ is the external load vector,
- $\Delta\lambda_i^{(j)}$ is the external load multiplier increment.

Since displacement discontinuities can be taken into account only at the interface between two elements, the crack trajectory not being generally known *a priori*, it proves necessary to modify a portion of the finite element mesh with each fictitious crack growth

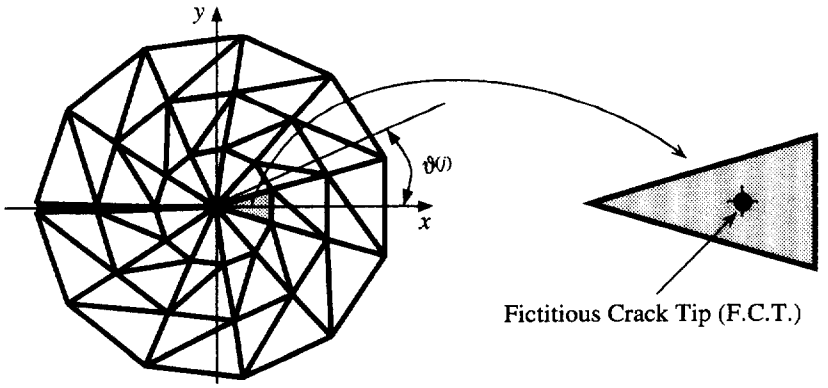

Fig. 3. The center of gravity of the dashed element is taken as the tip of the fictitious crack.

step. This is achieved through the rotary-translation motion of a finite element rosette (Figs 3 and 4) resulting in the automatic generation of a portion of the mesh.

Let us now examine the inner iterative cycle, omitting superscript j for the sake of simplicity. If the $\mathbf{L}_i$ matrix is non-singular, we get:

$$\left(\frac{\partial \mathbf{u}}{\partial \lambda}\right)_i = \mathbf{L}_i^{-1}\mathbf{F}. \tag{4}$$

Having worked out strain values from the displacements and by applying the constitutive law, it becomes possible to calculate $(\partial\sigma/\partial\lambda)_i$.

The cohesive model assumes that the fictitious crack spreads perpendicularly to the principal tensile stress ($\sigma_{F.C.T.}$) at the point where the latter reaches the tensile strength of the material, σ_u. At this point, referred to as fictitious crack tip (F.C.T.), the following equation applies:

$$\sigma_{F.C.T.} = \left(\frac{1}{2}(\sigma_x+\sigma_y)+\frac{1}{2}\sqrt{(\sigma_x-\sigma_y)^2+4\tau_{xy}^2}\right)_{F.C.T.} = \sigma_u. \tag{5}$$

The nonlinear equations governing the growth of real and fictitious cracks are solved through the following iterative cycle:

$$\begin{aligned}
&\left(\frac{\partial \sigma_{F.C.T.}}{\partial \lambda}\right)_i \mathrm{d}\lambda_{i+1} = \sigma_u - \sigma_{F.C.T.}(\mathbf{u}_i) \quad \text{(fictitious crack growth condition)}\\
&\Delta\lambda_{i+1} = \Delta\lambda_i + \mathrm{d}\lambda_{i+1}\\
&\mathbf{u}_{i+1} = \mathbf{u}_i + \mathbf{L}_i^{-1}\,\mathrm{d}\lambda_{i+1}\mathbf{F}\\
&(\ell_r)_{i+1} = f(\mathbf{u}_{i+1}) \quad \text{(real crack growth condition).}
\end{aligned} \tag{6}$$

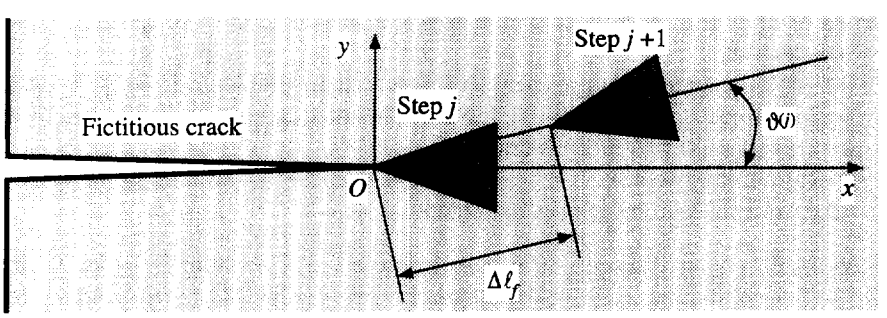

Fig. 4. Two consecutive positions of the fictitious crack tip.

ℓ_r is used to refer to the length of one of the real cracks during the initial stage of the iterative cycle, and to the length of the other crack during a subsequent stage.

For the problems examined it was found that the results do not change regardless of the order with which the two real cracks are considered. At each increment in the i indicator, only one cohesive connection is released. At the end of the iterative cycle (6) the following two conditions must be verified:

$$\sigma_{pt} \leqslant \sigma_u \quad \text{everywhere in the solid} \tag{7}$$

$$\dot{w}_n \geqslant 0 \quad \text{for } \ell_{r1} < s_1 \leqslant \ell_{f1} \text{ and } \ell_{r2} < s_2 \leqslant \ell_{f2}. \tag{8}$$

where σ_{pt} stands for the principal tensile stress. Should condition (8) be violated along one of the two cracks, the iterative cycle (6) must be repeated taking into account the possibility of rigid unloading along the crack which tends to close.

The lengths of the fictitious cracks (ℓ_{f1} and ℓ_{f2}) are surely increasing monotone functions of time during the irreversible process of crack growth. Consequently (Carpinteri and Valente, 1988) the variable ℓ_f, relating to cracks that are able to propagate, is taken as the control variable, and hence is increased by $\Delta\ell_f$ (Fig. 4) in the direction chosen according to the maximum principal tensile stress criterion:

$$\vartheta^{(j)} = \frac{1}{2}\arctan\left(\frac{2\tau_{xy}}{\sigma_x - \sigma_y}\right)^{(j)}. \tag{9}$$

3. NUMERICAL SIMULATION OF FOUR-POINT SHEAR TESTS

The experimental setup used for four-point shear tests is shown in Fig. 5 (Ferrara and Morabito, 1989). The related restraint and loading conditions are illustrated in Fig. 6, together with the finite element mesh used in numerical simulations (Schlangen and van Mier, 1991; Carpinteri *et al.*, 1993).

The material and geometric properties are listed in Table 1.

Since each specimen has a single notch, only the crack originating at the tip of the notch will propagate at first. The evolution of the principal tensile stress at point A (σ_A) of Fig. 6 (i.e. the point where the secondary crack is triggered) is plotted in Fig. 7 as a function of the length of the primary fictitious crack ($\ell_{r2} = \ell_{f2} = 0$).

The diagram in Fig. 7 shows a marked size effect on σ_A. It can be seen, in fact, that the opening of a secondary crack may be triggered below a critical size. This size effect was confirmed experimentally in the above-mentioned investigation (Ferrara and Morabito, 1989; Schlangen and van Mier, 1991; Carpinteri *et al.*, 1993) which showed that all specimens with $H = 0.1$ m broke in three pieces upon the opening of a secondary crack, whilst all specimens with $H = 0.2$ or 0.3 m split in two, as illustrated in Figs 8, 9, and 13.

In this connection it should be noted that the growth of a crack, in a brittle and heterogeneous material such as concrete, is the outcome of a process of coalescence of the microcracks existing in the material before the application of the load. The presence of a notch gives rise to a singularity in the state of stress which facilitates crack formation. Conversely, the absence of notches involves a 35–45% increase in tensile stress, resulting in the appearance of a crack. In this connection, Fig. 7 shows that, by increasing σ_u by 40%, we obtain a critical size (H) comprised between 0.1 and 0.2 m, in good agreement with the experimental findings.

Let us now consider the case $H = 0.1$ m, involving the propagation of two cracks, in both the theoretical model and in experimental reality. Figure 10 illustrates the evolution of ℓ_{f1} and ℓ_{f2} as a function of the index j for the external cycle.

From this diagram, it can be seen that, with $j \leqslant 6$ at the initial stage, the primary crack propagates (from the notch); during a subsequent stage, with $6 < j < 14$, the secondary crack spreads out from point A of Fig. 6. A third stage ($14 \leqslant j < 35$) is characterised by the simultaneous growth of both cracks. Finally, only the primary crack propagates during

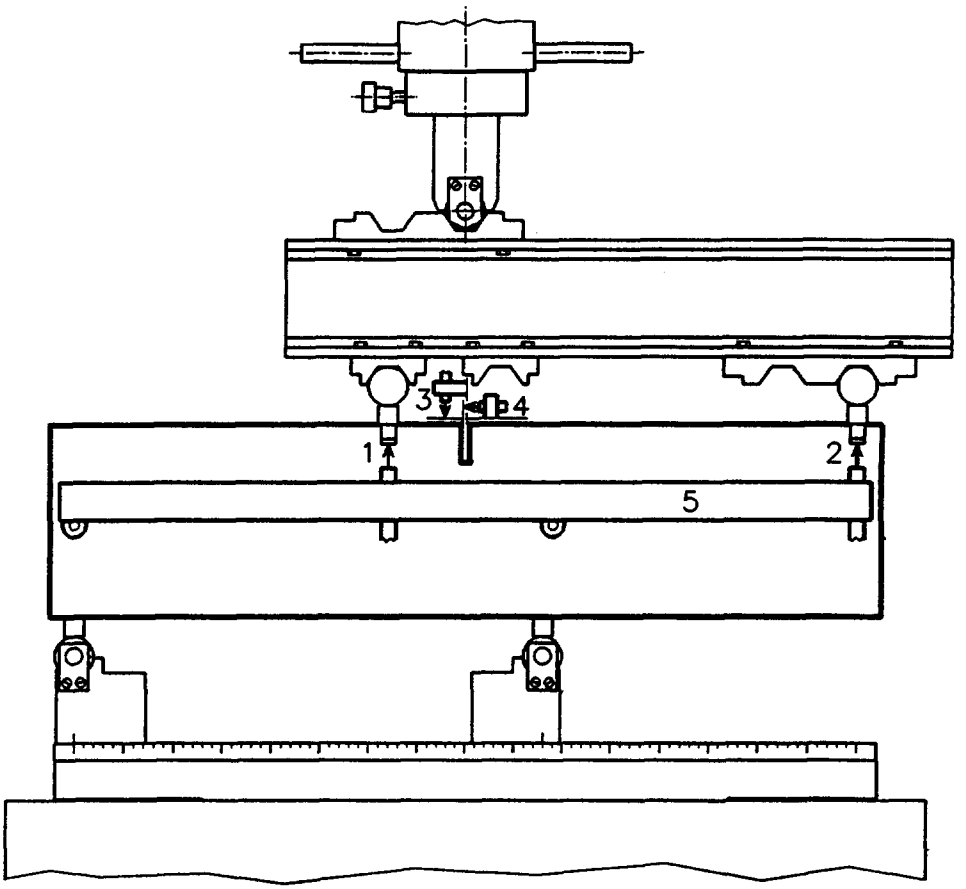

1: LVDT for the measurement of δ_1 deflection.

2: LVDT for the measurement of δ_2 deflection.

3: LVDT for the measurement of crack mouth sliding displacement (C.M.S.D.).

4: LVDT for the measurement of crack mouth opening displacement (C.MO.D.).

5: Reference bar for δ_1 and δ_2 measurement

Fig. 5. Experimental setup for four-point shear test.

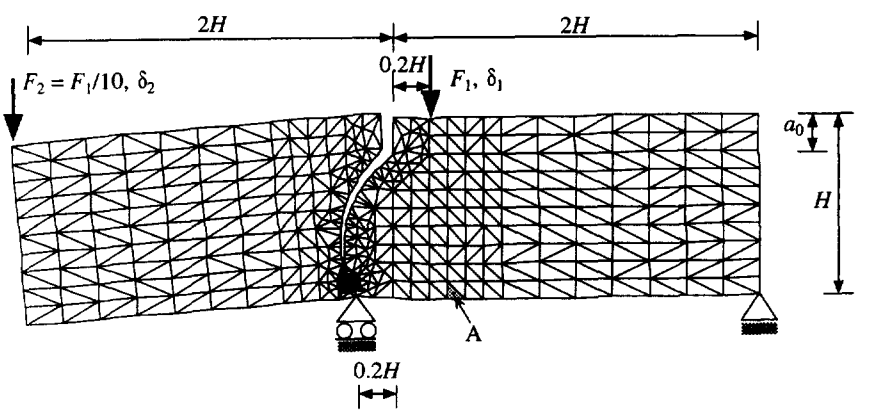

Fig. 6. Mesh used for the four-point shear test.

Table 1. Material and geometric properties

Thickness (t) (m)	a_0/H	$\Delta\ell_f$	E (MPa)	ν	σ_u (MPa)	$\mathcal{G}_F$ (N/m)
0.1	0.2	$H/50$	28,000	0.1	2.4	122

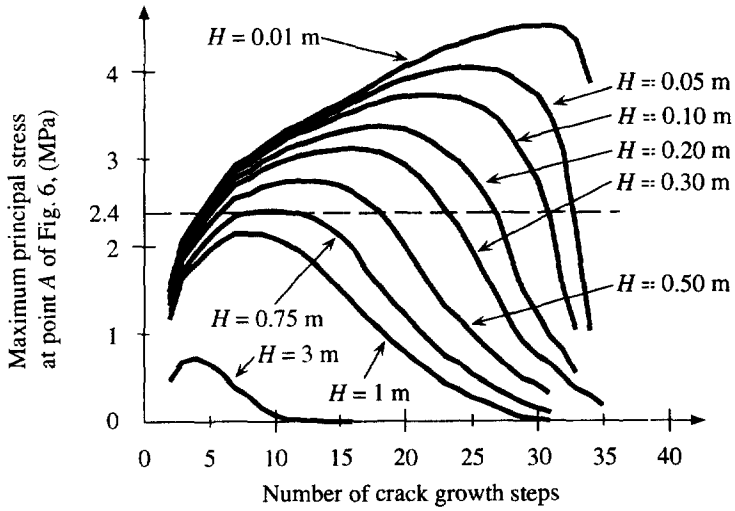

Fig. 7. Principal tensile stress at point A of Fig. 6 as a function of ℓ_{f1}. Single crack case ($\ell_{f2} = 0$).

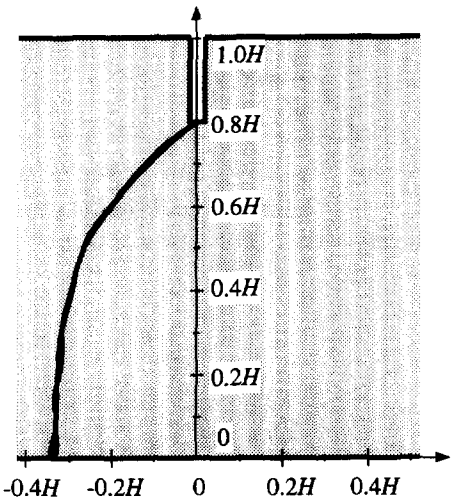

Fig. 8. Crack trajectories for $H = 0.2$ m (test results from Carpinteri *et al.*, 1993).

a final stage ($j \geqslant 35$) simulated numerically. The analysis is interrupted when the finite element rosette relating to the primary crack reaches the specimen's lower edge (Fig. 11).

The two smallest eigenvalues (α_1 and α_2) of $\mathbf{L}$ are plotted as a function of j in Fig. 12. They approach zero simultaneously, for $j = 36$. Immediately before this happens, two incremental solutions are possible in static and kinematic terms: with the first solution, the primary crack grows and the secondary one stops propagating; with the other solution the opposite is true. In this case, the choice must be made according to the maximum energy release rate criterion. Since this criterion leads to the selection of the first solution, whereby the secondary crack freezes, α_1 and α_2 display a sudden increase, following a change of sign of α_1 alone.

During the following steps, the application of the maximum energy release rate criterion always entails the growth of the primary crack only. Table 1 indicates that a value of

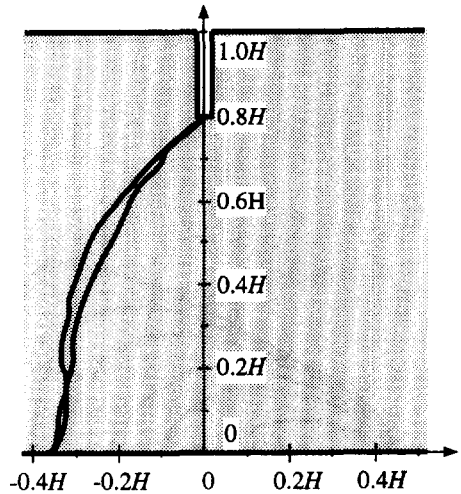

Fig. 9. Crack trajectories for $H = 0.3$ m (test results from Carpinteri *et al.*, 1993).

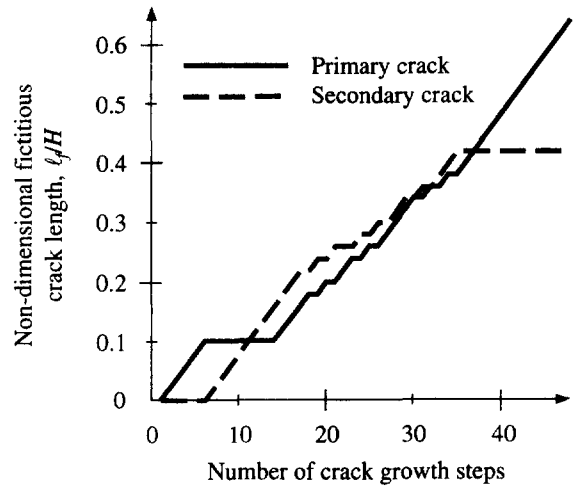

Fig. 10. Length of the two fictitious cracks (ℓ_{f1} and ℓ_{f2}) as a function of the number of crack growth steps.

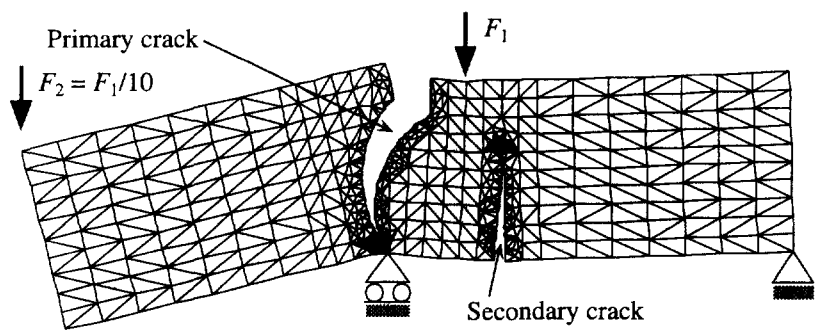

Fig. 11. Field of the total displacement corresponding to the last step of the numerical analysis (displacements magnified 150 times).

$\Delta\ell_f = H/50$ was used in the computations. In order to analyse how sensitive the predictions are to this assumed value, the numerical simulations were repeated, assuming $\Delta\ell_f = H/40$. The crack trajectories (Fig. 13), the diagrams of total load vs crack mouth opening displacements (Fig. 14) and total load vs crack mouth sliding displacements (Fig. 15) remain the same. As shown in Fig. 10, the secondary crack stops growing when its fictitious length reaches the value of 0.41 H. During the following steps, a local unloading condition occurs on the secondary crack. Since a rigid unloading hypothesis is assumed, the opening

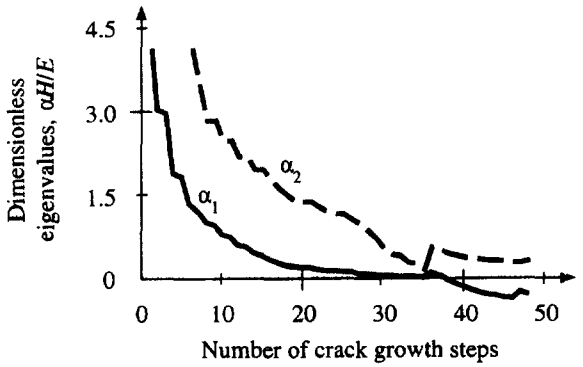

Fig. 12. The two smallest eigenvalues of L vs the number of crack growth steps.

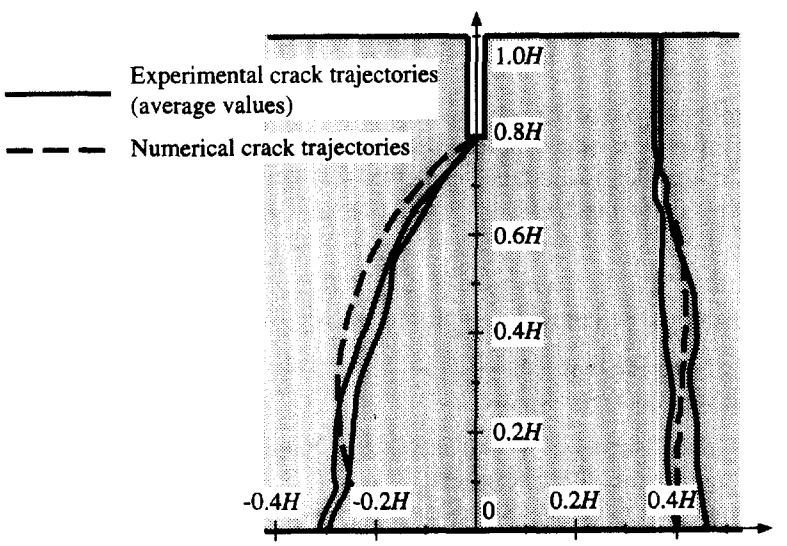

Fig. 13. Comparison between experimental and numerical crack trajectories, for the specimen sized $H = 0.1$ m.

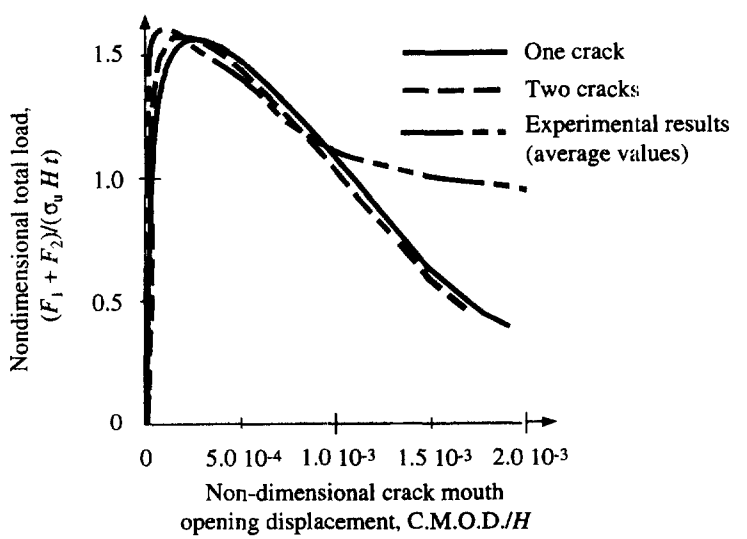

Fig. 14. Total load vs crack mouth opening displacement, for the specimen sized $H = 0.1$ m.

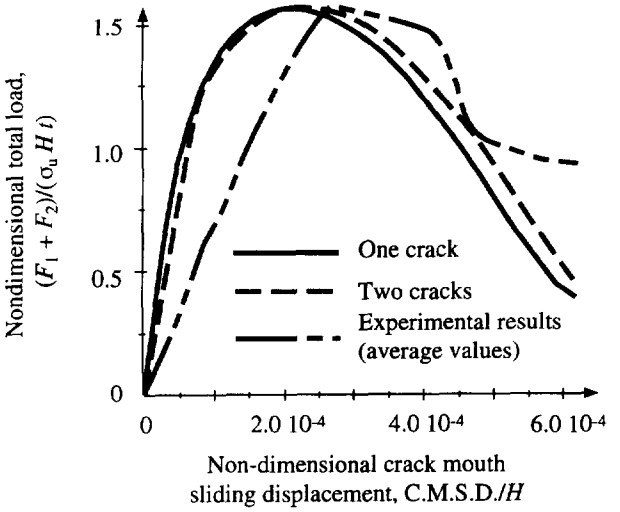

Fig. 15. Total load vs crack mouth sliding displacement, for the specimen sized $H = 0.1$ m.

displacement of the secondary crack remains constant during these steps. This displacement is the most sensitive response: it increases by 6% when $\Delta\ell_f$ is increased from $H/50$ to $H/40$. At the present it is difficult to establish whether this sensitivity is due to numerical reasons (mesh sensitivity) or to mechanical reasons (loss of uniqueness of solution due to strain softening).

4. COMPARISON BETWEEN NUMERICAL AND EXPERIMENTAL RESULTS

Figure 16 shows the diagrams of F_1, δ_1 and F_2, δ_2 for a specimen sized $H = 0.1$ m. In this connection we may observe that:

(1) Numerical models with one or two cracks give roughly the same maximum load, which is in good agreement with test results.
(2) The experimental deflection values δ_1 and δ_2 are measured with reference to a stiff bar, denoted with number 5 in Fig. 5. With this experimental setup, local deformation effects at the lower restraints do not modify δ_1 and δ_2. On the contrary the scheme used for the numerical simulations (Fig. 6) shows that δ_1 and δ_2 are computed with reference

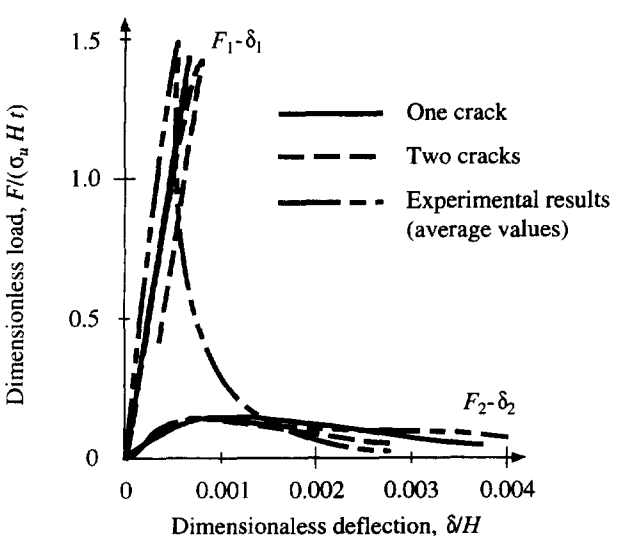

Fig. 16. F_1, δ_1 and F_2, δ_2 diagrams for the specimen sized $H = 0.1$ m. Comparison between theoretical and experimental results.

to the supports. Probably for this reason, both numerical models display greater deformability.

(3) The numerical model involving a single crack shows that the post-peak portion in the F_1–δ_1 diagram coincides with the pre-peak portion. Experimental reality is approximated more closely by the F_1–δ_1 diagram obtained through the numerical model involving two cracks. In the latter model, in fact, the post-peak portion is distinguishable from the pre-peak portion.

(4) Numerical and test results both show an F_2–δ_2 diagram with no snap-back. Accordingly, the δ_2 displacement is taken as the control variable in laboratory tests.

5. CONCLUSIONS

(1) From the four-point shear tests carried out (on specimens with a single notch) it can be seen that there is a critical size below which a secondary crack starts to propagate. This is a size-related phenomenon of bifurcation of the equilibrium path, which is predicted by the cohesive crack model and confirmed experimentally.

(2) When several solutions are possible from the static and kinematic point of view, the one corresponding to maximum energy release rate is chosen.

(3) The cohesive model involving two cracks approximates more closely the F_1–δ_1 diagram obtained experimentally, compared to the single crack version of the same model.

(4) Figures 13–16 show that theoretical and experimental results are in good agreement.

REFERENCES

Barenblatt, G. I. (1959) The formation of equilibrium cracks during brittle fracture: general ideas and hypotheses. Axially-symmetric cracks. *Journal of Applied Mathematics and Mechanics* **23,** 622–636.

Bazant, Z. P. and Cedolin, L. (1991) *Stability of Structures: Elastic, Inelastic, Fracture and Damage Theories.* Oxford University Press, Oxford.

Bocca, P., Carpinteri, A. and Valente, S. (1991) Mixed-mode fracture of concrete. *International Journal of Solids and Structures* **27,** 1139–1153.

Carpinteri, A. (1985) Interpretation of the Griffith instability as a bifurcation of the global equilibrium. In *Application of Fracture Mechanics to Cementitious Composites* (ed.) S. P. Shah, pp. 284–316. Martinus Nijhoff, The Netherlands.

Carpinteri, A. (1989) Size effects on strength, toughness and ductility. *Journal of Engineering Mechanics A.S.C.E.* **7,** 1375–1392.

Carpinteri, A. and Valente, S. (1988) Size-scale transition from ductile to brittle failure: a dimensional analysis approach. In *Cracking and Damage* (eds) J. Mazars and Z. P. Bazant, pp. 477–490. Elsevier Applied Science, Oxford.

Carpinteri, A., Valente, S., Ferrara, G. and Imperato, L. (1992) Experimental and numerical fracture modelling of a gravity dam. In *Fracture Mechanics of Concrete Structures* (ed.) Z. P. Bazant, pp. 351–360. Elsevier Applied Science, Oxford.

Carpinteri, A., Valente, S., Ferrara, G. and Melchiorri, G. (1993) Is mode II fracture energy a real material property? *Computers and Structures* **48,** 397–413.

Drucker, D. C. (1988) Conventional and unconventional plastic response and representation. *Applied Mechanics Review* **4,** 151–167.

Dugdale, D. S. (1960) Yielding of steel sheets containing slits. *Journal of Mechanics and Physics of Solids* **8,** 100–104.

Ferrara, G. and Morabito, P. (1989) A contribution of the holographic interferometry to studies on concrete fracture. In *Fracture of Concrete and Rock* (eds) S. P. Shah, S. E. Swartz, B. Barr, pp. 337–346. Elsevier Applied Science, Oxford.

Hillerborg, A., Modeer, M. and Petersson, P. E. (1976) Analysis of crack formation and crack growth in concrete by means of fracture mechanics and finite elements. *Cements and Concrete Research* **6,** 773–782.

Maier, G. (1971) Incremental plastic analysis in the presence of large displacements and physical instabilizing effects. *International Journal of Solids and Structures* **7,** 345–372.

Maier, G., Zavelani, A. and Dotreppe, J. C. (1973) Equilibrium branching due to flexural softening. *Journal of Engineering Mechanics A.S.C.E.* **89,** 897–901.

Nemat-Nasser, S., Sumi, Y. and Keer, L. M. (1980) Unstable growth of tension crack in brittle solids: stable and unstable bifurcations, snap-through, and imperfection sensitivity. *International Journal of Solids and Structures* **16,** 1017–1035.

Nguyen, Q. S. (1987) Bifurcation and post-bifurcation analysis in plasticity and brittle fracture. *Journal of Mechanics and Physics of Solids* **35,** 303–324.

Schlangen, E. and van Mier, J.G.M. (1991) Boundary effect in mixed mode I and II fracture of concrete. In *Proceedings of the International R.I.L.E.M./E.S.I.S. Conference on Fracture Processes in Brittle Disordered Materials: Concrete, Rock, Ceramics* (eds) J. G. M. van Mier, J. G. Rots, A. Bakker, Noordwijk, The Netherlands, pp. 705–716.